Available online at www.sciencedirect.com
SCIENCE DIRECT
Journal of Photochemistry and Photobiology A: Chemistry 180 (2006) 322–327
Journal of Photochemistry and Photobiology A:Chemistry
www.elsevier.com/locate/jphotochem

Laser pulse control of exciton dynamics in the FMO complex: Polarization shaping versus effects of structural and energetic disorder

Ben Brüggemann [a,*], Tõnu Pullerits [a], Volkhard May [b]

[a] *Department of Chemical Physics, Lund University, P.O. Box 124, SE-22100 Lund, Sweden*
[b] *Department of Physics, Humboldt University at Berlin, Newtonstr. 15, D-12489 Berlin, Germany*

Available online 11 April 2006

Abstract

Femtosecond laser pulse control of exciton dynamics in biological chromophore complexes is studied theoretically using the optimal control theory specified to open quantum systems. Based on the laser pulse induced formation of an excitonic wave packet the possibility to localize excitation energy at a certain chromophore within a photosynthetic antenna system (FMO complex of green bacteria) is investigated both for linearly polarized and polarization shaped pulses. Results are presented for an ensemble of N energetically disordered and randomly oriented FMO complexes. Here, the optimized control pulse represents a compromise with respect to the solution of the control task for any individual complex of the ensemble. For the case of an ensemble with $N = 10$ members the polarization shaped control pulse leads to a higher control yield compared with a linearly polarized pulse. This difference becomes considerably smaller for an ensemble with $N = 120$ members. The respective optimized pulses are used to drive excitation energy in a different ensemble with $M \gg N$ complexes to simulate the usual experimental condition in solution. For the case with $N = 120$, the relative control yield coincides with the resulting control yield "in solution", giving a slightly higher control yield for polarization shaped pulses.

Keywords:
Optimal control; Exciton; Photosynthetic antenna system; FMO; Exciton control; Polarization

1. Introduction

The combination of femtosecond laser pulse shaping with a closed-loop feedback arrangement represents an experimental breakthrough in realizing the control of molecular dynamics and chemical reactions by light (cf., for example, Ref. [1] and the recent attempt to trigger conformational changes in Ref. [2]). Todays pulse shaping technology allows for a simultaneous and independent manipulation of the two different polarization directions of the laser beam [3]. If in the course of optical excitation the spatial direction of the electric-field vector can be adapted to the transition dipole moment orientation we may expect a considerable increase of the control yield. However, random orientations of the molecules in solution may drastically reduce this effect.

In the following we will investigate the potential of the polarization control in comparison to a control task with linearly polarized light only (some preliminary results have been already presented in Ref. [4]). A well suited example is given by the control of excitation energy dynamics in spatially non-regular chromophore complexes like photosynthetic antenna systems. This has already been demonstrated by us for the FMO complex [5] and the PS1 [6]. The particular control aim there has been the excitation energy localization at a single chromophore at a definite time. This requires the photo induced formation of an excitonic wave packet, i.e., the time-dependent superposition $\sum_\alpha A_\alpha(t)|\alpha\rangle$ of the various exciton states $|\alpha\rangle$ in such a way that at the final time t_f of the control task the superposition corresponds to excitation energy localization at a particular chromophore m, i.e., $\sum_\alpha A_\alpha(t = t_f)|\alpha\rangle = |m\rangle$. Here, we also indicate that it would be of interest to study the more realistic case of a distribution of the time to reach the target state, say, ± 10 fs around t_f [7]. However, since the exciton dynamics in the FMO complex are rather slow on a 20 fs time-scale such a target state delocalized in time would not change the outcome much.

Our simulations of exciton localization in the PS1 core antenna [6] have shown that the control efficiency is strongly temperature dependent, and that for each temperature a different op-

* Corresponding author. Tel.:+46 46 2228131; fax: +46 46 2224119.
E-mail address: ben.bruggemann@chemphys.lu.se (B. Brüggemann).

1010-6030/$ – see front matter © 2006 Elsevier B.V. All rights reserved.
doi:10.1016/j.jphotochem.2006.02.026

timal pulse length exists. Furthermore, for the FMO complex, the influence of higher excited states and of exciton–exciton annihilation could be discussed, also including a first account for random complex orientation and energetic inhomogeneity [5]. There exists also an experimental demonstration of energy transfer control in the photosynthetic antenna LH2 by guiding excitation energy between carotenoids and bacteriochlorophylls [8,9].

To form the superposition state $\sum_\alpha A_\alpha(t)|\alpha\rangle$ all exciton states in a control task have to be addressed, therefore the oscillator strength should be distributed over all exciton states $|\alpha\rangle$ what excludes the use of highly symmetric complexes for such studies. For an appropriate non-regular structure, however, different transition dipole moments $\mathbf{d}_\alpha$ may also posses different spatial orientations. Having a polarization shaped field $\mathbf{E}(t)$, the spatial orientation of $\mathbf{E}(t)$ (perpendicular to the propagation direction) represents an additional degree of freedom. It increases the flexibility for putting the various coupling expressions $\mathbf{d}_\alpha\mathbf{E}(t)$ in the right order of magnitude at the right time interval to finally achieve the proper wave packet formation.

This will be demonstrated in using a theoretical description in terms of a density matrix version of the optimal control theory (OCT) [10–12]. In continuing our computations of Ref. [5] we aim at localizing an excitonic wave packet at a certain chromophore in the FMO complex. The FMO complex is particularly suited because it contains only seven bacteriochlorophylls (BChls) as chromophores with a well-defined energy and spatial position [13,14]. However, the chromophores of the FMO complex exhibit energetic disorder. And, since they are investigated as isolated particles in solution, one has also account for their random orientations. Therefore, it will be a particular challenge to find out whether or not polarization shaping may compensate the control yield reduction originated by disorder.

The paper is structured as follows. First the exciton model of the FMO complex and the related density matrix approach are shortly explained. Afterwards, OCT is used to calculate the optimized excitation pulses accounting for polarization shaping as well as the effect of disorder in an ensemble of FMO complexes. Up to 120 energetically disordered and randomly oriented FMO complexes are considered simultaneously in Section 3.1. In the last section we compare the control achievements of several optimized pulses with those obtained on a much larger ensemble of FMO complexes in order to imitate a typical experimental setting.

2. Theory

2.1. Exciton model

Exciton models for photosynthetic antennae like the FMO complex are well established (see, e.g., Refs. [15–17]). Each chromophore at site m is modeled as a two level system (ground-state and Q_y-state) with the respective excitation energy ε_m and the transition dipole moment μ_m oriented according to the spatial structure of the complex (cf. Fig. 1). The Coulombic interaction V_{mn} among different chromophores of the FMO complex (responsible for excitation energy transfer) can be approximated as a dipole–dipole coupling. For all quantities mentioned so far we use values suggested in Ref. [14]. It suffices for the present purposes to concentrate on the state $|0\rangle$ where all molecules are in their ground-state, and on the states $|m\rangle$ with the single chromophore m excited. Diagonalizing the Hamiltonian of these singly excited states leads to the (single) exciton states $|\alpha\rangle = \sum_m C_\alpha(m)|m\rangle$, with energies ε_α (for a more involved discussion, also including two-exciton states see Refs. [5,18,16]). Exciton–vibrational coupling is obtained by accounting for a modulation of the ε_m and V_{mn} by intra- and inter-chromophore vibrations as well as those of the protein matrix (for details see Refs. [16,17]).

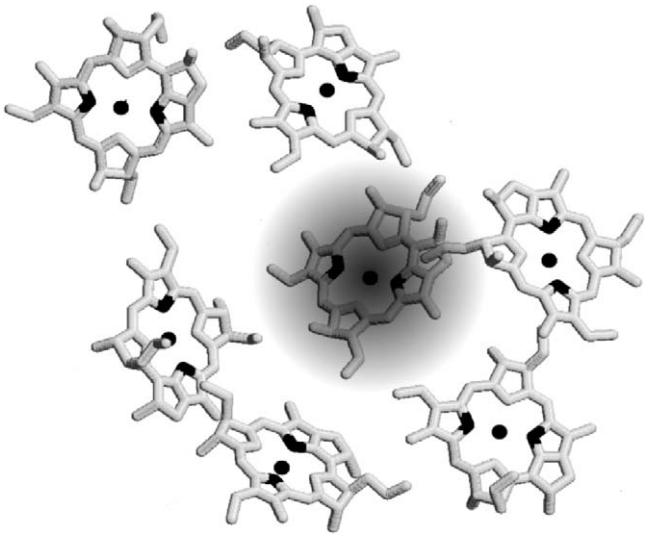

Fig. 1. Arrangement of the seven BChls in the FMO complex of *Prosthecochloris aestuarii* [13] (identifier 4BCL in the Protein Data Bank). The atoms in the line of the respective Q_y dipole moments are plotted in black (using rasmol). At the end of the control pulse, the exciton should be localized at the central chromophore, thus acting as the target chromophore.

2.2. Density matrix theory

Since the exciton–vibrational coupling in the FMO complex is relatively weak, the whole set of vibrations can be handled as a reservoir staying in thermal equilibrium independent on the actual excitation of the chromophores. Thus, it is possible to account for the resulting effects of excitonic energy dissipation and dephasing in the framework of a density matrix theory. It is based on the introduction of the reduced exciton density operator $\hat{\rho}$ and a perturbative treatment of the coupling to the reservoir. We apply the so-called Markov and Bloch approximation [5,18,16,17] and write the related equation of motion for $\hat{\rho}$ as

$$\frac{\partial}{\partial t}\hat{\rho}(t) = -i\left(\mathcal{L}_0 - i\mathcal{D} + \mathcal{L}_{\text{field}}\right)\hat{\rho}(t). \tag{1}$$

The superoperators $\mathcal{L}_0$, $\mathcal{D}$ and $\mathcal{L}_{\text{field}}$ account for the free evolution of excitons, for dissipation and for the coupling to the radiation field, respectively. Related density matrix equations follow by changing over to the exciton density matrix $\rho_{\tilde{\alpha}\tilde{\beta}} = \langle\tilde{\alpha}|\hat{\rho}(t)|\tilde{\beta}\rangle$ (in this notation, e.g., $\tilde{\alpha}$ can stand either for an exciton state or for the ground state of the complex). Then, the diagonal elements

of the density matrix give the populations $P_{\tilde{\alpha}}$ (of the exciton states or the ground-state). The free time evolution is simply determined by $\langle\tilde{\alpha}|\mathcal{L}_0\hat{\rho}|\tilde{\beta}\rangle = \Omega_{\tilde{\alpha}\tilde{\beta}}\rho_{\tilde{\alpha}\tilde{\beta}}(t)$ with $\hbar\Omega_{\tilde{\alpha}\tilde{\beta}} = \varepsilon_{\tilde{\alpha}} - \varepsilon_{\tilde{\beta}}$ (note $\varepsilon_{\tilde{\alpha}=0} = 0$). The action of the dissipative superoperator $\mathcal{D}$ (related to excited states $\tilde{\alpha} = \alpha$) is obtained as

$$\langle\alpha|\mathcal{D}\hat{\rho}|\beta\rangle = \delta_{\alpha\beta}\sum_{\gamma}(k_{\alpha\to\gamma}\rho_{\alpha\alpha} - k_{\gamma\to\alpha}\rho_{\gamma\gamma}) + \frac{1}{2}(1-\delta_{\alpha\beta})\sum_{\gamma}(k_{\alpha\to\gamma} + k_{\beta\to\gamma})\rho_{\alpha\beta}. \quad (2)$$

The quantities $k_{\alpha\to\beta}$ are rate constants for exciton energy relaxation via a transition from state $|\alpha\rangle$ to state $|\beta\rangle$. They read

$$k_{\alpha\to\gamma} = 2\pi\Omega_{\alpha\gamma}^2(1+n(\Omega_{\alpha\gamma}))\sum_{m}|C_\alpha(m)C_\gamma(m)|^2(J(\Omega_{\alpha\gamma}) - J(-\Omega_{\alpha\gamma})), \quad (3)$$

where $n(\Omega)$ denotes the Bose–Einstein distribution and J is the spectral density of the coupling to the reservoir vibrations identical for each chromophore. The special form $J(\omega) = j\omega^2\sum_{\nu=1}^{5}1/2\omega_\nu^3 \times \exp(-\omega/\omega_\nu)$ used in the following has been deduced from fluorescence measurements [19,20]. Finally, the coupling to the radiation field $\mathcal{L}_{\text{field}}$ is simply obtained via the commutator with the coupling expressions $-\mathbf{E}(t)\hat{\mu}$ (where $\hat{\mu}$ is the overall dipole operator of the complex).

2.3. Polarization shaping and account for disorder in optimal control theory

Within OCT one computes the temporal behavior of the field $\mathbf{E}(t)$ which drives the system into the chosen target state. With regard to the experimental setup, the result of the OCT would correspond to a phase and amplitude shaped pulse. In the present case $\mathbf{E}(t)$ is obtained by a maximization of the population of the target state $|m\rangle$. This requires to maximize $P_m(t) = \langle m|\hat{\rho}(t)|m\rangle$ at the constraint of a finite laser pulse intensity (the matrix elements of the density operator in the basis of localized excitations can be easily computed from the $\rho_{\alpha\beta}$). The demand of maximizing P_m results in the following functional equation for the temporal behavior of the optimal pulse field-strength [5,10,12]:

$$\mathbf{E}(t) = \frac{i}{\hbar\lambda(t)}\text{tr}\{\hat{\sigma}(t;\mathbf{E})\,[\hat{\mu},\,\hat{\rho}(t;\mathbf{E})]\}. \quad (4)$$

Here, $\lambda(t)$ is the Lagrange parameter of OCT, whose time dependency assures that the pulse is switched on and off smoothly at t_0 and t_f, respectively (its integrated value is related to the field intensity in a nonlinear way [5]). Besides $\hat{\rho}$, the trace in Eq. (4) (to be taken with respect to the ground-state and all single exciton states) also includes the auxiliary density operator $\hat{\sigma}$ which has to be propagated backwards in time by an equation which appears as a slight modification of Eq. (1) and with the "initial value" $\hat{\sigma}(t_\text{f}) = |m\rangle\langle m|$ [21] (see also Refs. [5,10,12]). The temporal evolution of both density operators is determined by the field $\mathbf{E}$ given explicitly by Eq. (4). Therefore, replacing $\mathbf{E}$ in $\mathcal{L}_{\text{field}}$ by the right-hand side of Eq. (4) one arrives at coupled nonlinear equations of motions for $\hat{\rho}$ and $\hat{\sigma}$. Their iterative solution solves the control task and results in an expression for the optimal pulse (provided that convergence has been achieved, for details see Ref. [5]).

If the radiation field which propagates in z-direction is linearly polarized, say in x-direction, Eq. (4) determines the related field amplitude E_x, and on the right-hand side the vectorial dipole operator has to be replaced by its x-component $\hat{\mu}_x$. To account for an independent variation of the two polarization directions of the radiation field we represent $\mathbf{E}$ by the field amplitude E_x in x-direction and E_y in y-direction. Then, a respective separation of Eq. (4) results in coupled functional equations for $E_x(t)$ and $E_y(t)$. Moreover, the expression in the equation of motion (1) for the density operator describing the coupling to the radiation field reads $-[E_x\hat{\mu}_x + E_y\hat{\mu}_y,\,\hat{\rho}]/\hbar$. In an experiment this approach would correspond to the shaping of amplitude and phase in x- and y-polarization separately.

The inclusion of energetic disorder (for example, the fluctuation of the chromophore excitation energies ε_m) and random spatial orientation is somewhat more involved [5]. Now, the laser pulse has to solve the control task for an ensemble of complexes where the individual complexes may differ one from another. Accordingly, the optimal pulse is determined by an expression similar to Eq. (4) but with an ensemble average on the right-hand side. If denoted either for the x- or the y-component of the field it reads

$$E_{x,y} = \frac{1}{N}\sum_{j=1}^{N}\frac{i}{\hbar\lambda(t)}\text{tr}\{\hat{\sigma}^{(j)}(t;\mathbf{E})[\hat{\mu}_{x,y}^{(j)},\,\hat{\rho}^{(j)}(t;\mathbf{E})]\}. \quad (5)$$

Here, we have to understand $\mathbf{E}$ at the right-hand side as $\mathbf{n}_x E_x + \mathbf{n}_y E_y$, and j counts the N different complexes of the ensemble. Also, the right-hand side includes the respective ensemble (configuration) average $1/N \times \sum_{j=1}^{N}\ldots \equiv \langle\ldots\rangle_{\text{config}}$. Moreover, the dipole operators $\hat{\mu}_x^{(j)}$ or $\hat{\mu}_y^{(j)}$ of the j-th complex appear as well as the two density operators $\hat{\rho}^{(j)}$ and $\hat{\sigma}^{(j)}$. Those have to be propagated according to equations like Eq. (1) but specified to the j-th complex of the ensemble. If E_x and E_y in the field-term of these equations of motion are replaced by the respective right-hand side of Eq. (5) all equations for $\hat{\rho}^{(j)}$ and $\hat{\sigma}^{(j)}$ are coupled one to another and have to be solved simultaneously. Usually, to arrive at a satisfactory disorder averaging, N has to be about 10^3 and larger [16]. This would make the computation rather expensive and a considerable reduction of N might be necessary.

3. Results and discussion

The theoretical approach of OCT shortly explained in the preceding section is used next to study laser pulse induced excitation energy localization at a particular chromophore of the (monomeric) FMO complex. All definitions and parameters used are directly comparable to our foregoing studies of Ref. [5]. In particular, the simulations are carried out at 4 K, and the final time t_f of the control task is put at 600 fs. The overall single-exciton population of the complexes $P_{\text{ex}} = \sum_\alpha \rho_{\alpha\alpha} = \sum_n P_n = (1 - P_0)$ has been limited to values of 0.25 ± 0.03 by a proper value of the Lagrange parameter $\lambda(t)$ in Eq. 5 [5]. This guarantees to stay in a linear excitation regime and justifies the

neglect of two and higher exciton states. In this connection it is advisable to renormalize the configuration averaged target state population to $\langle P_{\mathrm{ex}}\rangle_{\mathrm{config}}$ as

$$P_m^{(\mathrm{ren})}(t) = \frac{\langle P_m(t)\rangle_{\mathrm{config}}}{\langle P_{\mathrm{ex}}(t)\rangle_{\mathrm{config}}}, \tag{6}$$

where $\langle P_m\rangle_{\mathrm{config}}$ denotes the configuration averaged excitation probability of chromophore m acting as the target chromophore. Independent on the degree of overall excitation the renormalized population tells us to which extend the excitation present among the single-exciton states arrived at the target state. For the configuration averaging, energetic disorder can be reduced to diagonal disorder with the single chromophore energies fluctuating independently about 100 cm^{-1} (full width at half maximum) around their mean value (similar to that what has been used in Ref. [14]). Moreover, random spatial orientations of the complexes have been assumed.

3.1. Laser pulse control for a disordered ensemble of complexes

We studied two types of ensembles, one with $N = 10$ complexes and one with $N = 120$. The first corresponds to an experiment close to the border of single-molecule spectroscopy. The larger ensemble should be related to an experiment done at a rather huge number of complexes. We assume here that the orientation and the energetic disorder of the single complexes does not change during the experiment. The restriction to $N = 120$, however, is dictated by the larger numerical effort necessary.

Fig. 2 shows the averaged site populations (the target state population $P_m^{(\mathrm{ren})}$ and all other site populations $P_{n\neq m}^{(\mathrm{ren})}$) together with the temporal behavior of the optimal pulses for $N = 10$. Using a linearly polarized optimal pulse (Fig. 2A), the average population of the central (target) chromophore in the FMO complex is coherently driven up to a level of 0.45, (cf. Ref. [5]). Compared to the population of about 0.7 that could be achieved for a properly oriented single FMO [5], the level of control is reduced. Now we enable polarization control, but leave all other parameters untouched. For a single complex, the target site population went up to 0.8 (not shown), and the optimization gain does not depend as much on the orientation as in the previous case. Using the same 10 complexes as before, the renormalized population of the target chromophore (also averaged, cf. Eq. (6)) reaches $P_m^{(\mathrm{ren})} = 0.55$ at the target time, which is less than in the case with only a single complex but more than what could be achieved with a linearly polarized pulse (Fig. 2B). A closer inspection of the resulting pulses reveals that the x-polarized and the y-polarized parts are shifted in phase by about 0.65π, thus leading to a mainly circularly polarized pulse.

The simulations discussed beforehand are repeated for a set of $N = 120$ complexes. Now, the control yield is further reduced, reaching $P_m^{(\mathrm{ren})} = 0.33$ for the linearly polarized pulse (Fig. 3A), and $P_m^{(\mathrm{ren})} = 0.34$ for the polarization shaped pulse (Fig. 3B). The phase shift between the x- and y-polarized parts of the pulse is about 0.55π, thus again giving a mostly circularly polarized pulse. The independence of the control yield on the concrete polarization of the laser pulse for a large ensemble is not astonishing. In such a case where really random orientation and Gaussian energy distribution is achieved the differences between linear and polarization shaped excitation is averaged out. The random orientation of the complexes does not favor a possible adaption of the polarization shaped pulse to the various excitonic transition dipole moments. However, the resulting circular polarization of the optimal pulse suggests that the circular dichroism (CD) of the FMO complex is addressed. Since its CD is small compared to the linear absorption (<1%) [14], the gain in control changing from linearly polarized to circularly polarized laser pulses is limited.

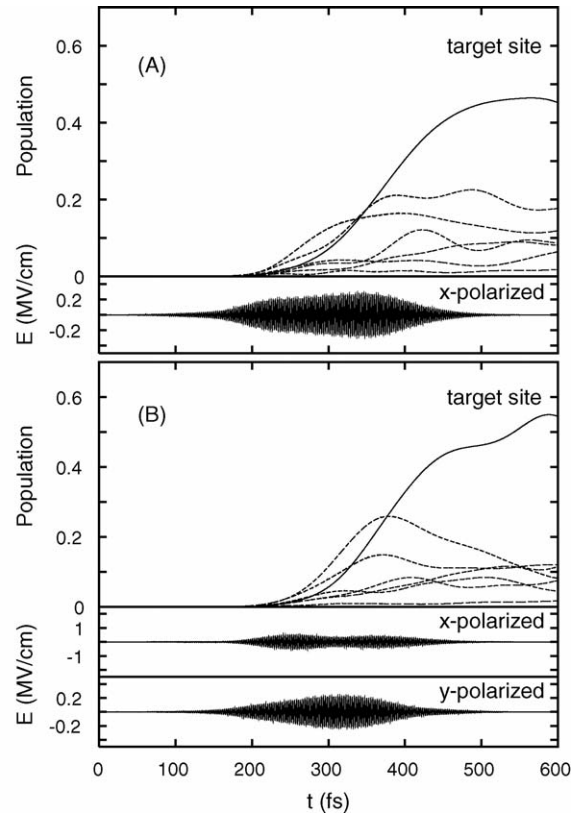

Fig. 2. Time evolution of the renormalized averaged populations $P_n^{(\mathrm{ren})}$ of the seven chromophores in a disordered ensemble of 10 FMO complexes after excitation with the optimal pulse (the target site population is displayed by the solid line, all other populations are shown by dashed lines, cf. Fig. 1). In case A (upper panel), the optimization was restricted to a linearly polarized pulse (see the lower section for the temporal behavior of the field-strength). In case B (lower panel), the optimization covered two polarization directions (see the lower section for the temporal behavior of both field-strengths).

3.2. Laser pulse control in the limit of a large ensemble of disordered complexes

The case of an ensemble with $N = 120$ complexes indicates the right tendency for an averaging with respect to a rather huge number of complexes. Nevertheless, statistical fluctuations are strong and results for $N \gg 120$ are of interest. This would also account for changes of orientation or energetic disorder during the measurement, since all possible orientations and energetic disorder distributions are already present. As the direct method

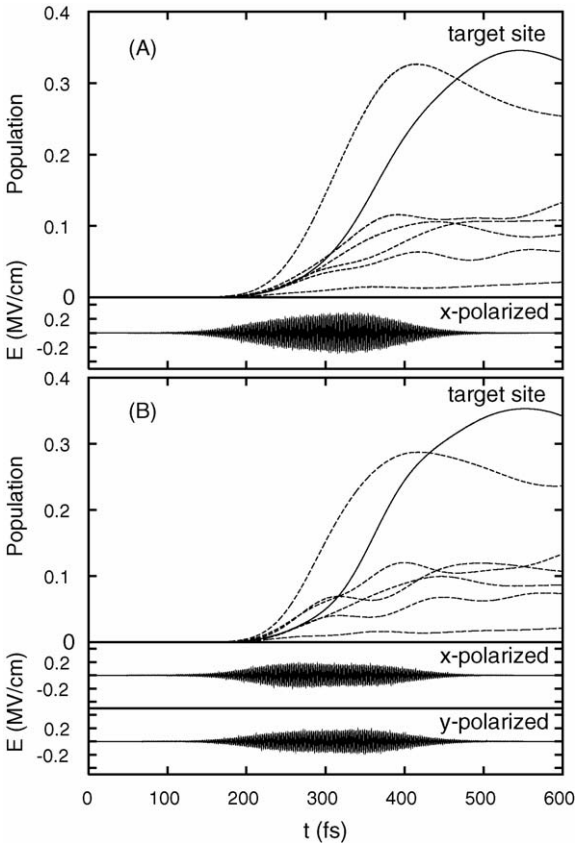

Fig. 3. Time evolution of the renormalized averaged populations $P_n^{(\mathrm{ren})}$ of the seven chromophores in a disordered ensemble of 120 FMO complexes after excitation with the optimal pulse (the target site population is displayed by the solid line, all other populations are shown by dashed lines, cf. Fig. 1). In case A (upper panel), the optimization was restricted to a linearly polarized pulse (see the lower section for the temporal behavior of the field-strength). In case B (lower panel), the optimization covered two polarization directions (see the lower section for the temporal behavior of both field-strengths).

of going to larger N is computationally too expensive, we proceed in a different way. We use the optimal pulses gained for control tasks at $N \leq 120$ and test their quality by driving FMO complexes of a much larger ensemble with $M \gg N$ complexes.

The result is given in Fig. 4A and B, for the linear and polarization shaped pulse, respectively. In each picture, the upper curve shows the renormalized population of the target chromophore in dependence on the number of complexes N in the completely controlled ensemble. The lower curve displays the renormalized target chromophore population at t_f averaged with respect to the "solvent ensemble" of $M = 5000$ complexes. The actual value of N indicates that the "solvent ensemble" has been driven by the optimal pulse already obtained for the N-ensemble. As a reference, a 200 fs (full width at half maximum) Gaussian pulse at 803 nm has been used. Due to its small bandwidth of 5 nm it excites mostly one specific exciton state, which is by 70% localized at the target chromophore (giving rise to a target site population of 0.30). As it is shown in the upper parts of Fig. 4A and B the two population values converge in both cases: to 0.33 for the linearly polarized pulse, and to the slightly higher value of 0.34 for the polarization shaped pulse, 10% and 13% higher than that for the reference pulse, respectively. The lines

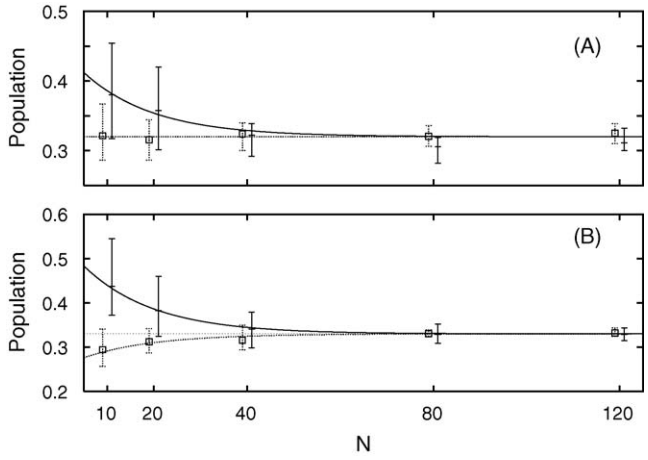

Fig. 4. Normalized averaged population $P_m^{(\mathrm{ren})}$ of the target chromophore in dependence on the number N of different FMO complexes in the ensemble (bars connected by a solid line). In the upper panel 'A', a linearly polarized laser pulse has been used, whereas for the lower panel 'B', polarization shaping was included. Additionally, the averaged normalized population of the target chromophore in a different ensemble of $M = 5000$ disordered complexes is displayed vs. N (squares connected by a dotted line). The respective values are computed in using the optimal pulse obtained for the actual value of N. Each simulation has been repeated three times, the mean value is shown, and the highest and lowest value are indicated by the error bars. The lines are fits using a single exponential.

are given by one exponential with the decay constants of $\nu \sim 15$ for all pulses. It is interesting to see that for the linearly polarized control pulse, even for the lowest number of $N = 10$ complexes in the completely controlled ensemble, some of the pulses give an excellent yield in the solvent ensemble. With larger N only the variance of the yields of the solvent ensemble for different optimal pulses gets smaller (Fig. 4A). However, for the polarization shaped pulses $N > 40$ is needed until the maximal yield for the solvent ensemble is consistently reached (Fig. 4B).

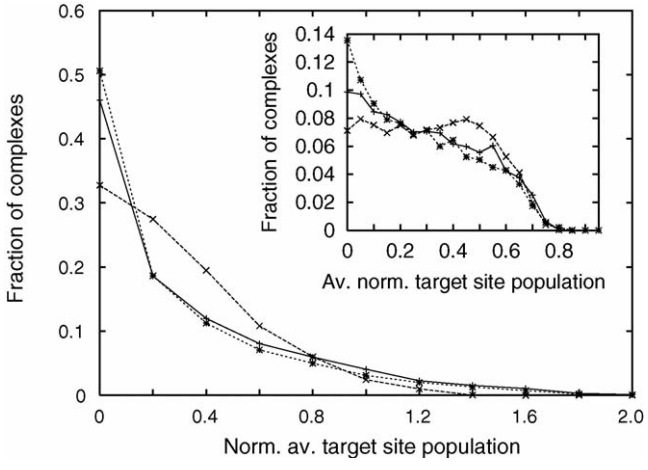

Fig. 5. Distribution of the averaged population $P_m^{(\mathrm{ren})}$ of the target chromophore in an ensemble of 5000 disordered complexes after excitation with the optimal pulse following from particular control tasks: use of a linear polarized pulse (case A), optimized for 120 complexes (solid curve,+). Polarization shaped pulse (case B), optimized for 120 complexes (dashed curve, ×). Gaussian pulse centered at the excitation energy of the target site (short dashed curve, stars). The inset displays the distribution of the averaged normalized population $\langle P_m / P_{\mathrm{ex}} \rangle_{\mathrm{config}}$ of the target chromophore for the same optimal pulses.

As a last topic we investigate how the distribution of the individual control yields $P_m^{(\mathrm{ren})}$ in the "solvent ensemble" changes between the optimized pulses of Fig. 3 ($N = 120$) and the reference pulse. The linearly polarized shaped pulse gives a similar yield distribution as the reference pulse, just slightly shifted towards higher values, whereas the polarization shaped pulse leads to a distribution which is more dominated by intermediate values of $P_m^{(\mathrm{ren})}$ (Fig. 5). The difference becomes even clearer if one changes to the relative yields with respect to the single complexes, $\langle P_m / P_{\mathrm{ex}} \rangle_{\mathrm{config}}$ (Fig. 5, inset).

4. Conclusion

The potential of polarization shaping in laser pulse control of excitation energy transfer in chromophore complexes has been demonstrated by energy localization at a single chromophore of the FMO complex. The level of control could be drastically enhanced by an optimal pulse consisting of an x- and y-polarized part if the disordered ensemble is small and consists of $N = 10$ FMO complexes. Such an enhancement becomes small for a larger ensemble of $N = 120$ complexes. Using the gained optimal pulses it turned out that for large N the control yield converges with the resulting control yield "in solution", at 0.33 for linearly polarized shaped pulses, and at 0.34 for polarization shaped pulses, 10–13% higher than that of a reference single wavelength Gaussian shaped pulse.

We conclude the need of rather small or ordered ensembles of chromophore complexes when trying to localize excitation energy. In such a case the control with polarization shaped pulses offers a big advantage. Once excitation energy localization with a sufficient control yield has been achieved one may systematically study different relaxation pathways starting with excitation energy localized at different chromophores.

Acknowledgments

Financial support by the DFG through Sfb 450 (V.M.) and the Swedish Research Council (B.B. and T.P.) is kindly acknowledged.

References

[1] A. Assion, T. Baumert, M. Mergt, T. Brixner, B. Kiefer, V. Seyfried, M. Strehle, G. Gerber, Science 282 (1998) 919–922.
[2] G. Vogt, G. Krampert, P. Nikolaus, P. Nuernberger, G. Gerber, Phys. Rev. Lett. 94 (2005) 068305.
[3] T. Brixner, G. Krampert, T. Pfeifer, R. Selle, G. Gerber, M. Wollenhaupt, O. Graefe, C. Horn, D. Liese, T. Baumert, Phys. Rev. Lett. 92 (2004) 208301.
[4] B. Brüggemann, T. Pullerits, V. May, in: W. Castleman (Ed.), Femtochemistry VII Procedings, Elsevier, 2006, in press.
[5] B. Brüggemann, V. May, J. Phys. Chem. B 108 (2004) 10529–10539.
[6] B. Brüggemann, V. May, Chem. Phys. Lett. 400 (2004) 573–577.
[7] A. Kaiser, V. May, J. Chem. Phys. 121 (2004) 2528;
A. Kaiser, V. May, Chem. Phys. 320 (2006) 95.
[8] J.L. Herek, W. Wohlleben, R.J. Cogdell, D. Zeidler, M. Motzkus, Nature 417 (2002) 533–535.
[9] W. Wohlleben, T. Buckup, J.L. Herek, M. Motzkus, Chem. Phys. Chem. 6 (2005) 850–857.
[10] Y. Ohtsuki, W. Zhu, H. Rabitz, J. Chem. Phys. 110 (1999) 9825–9832.
[11] T. Mancal, V. May, Eur. Phys. J.D. 14 (2001) 173–184.
[12] T. Mancal, U. Kleinekathöfer, V. May, J. Chem. Phys. 117 (2002) 636–646.
[13] D.E. Tronrud, B.W. Matthews, J. Deisenhofer, J.R. Norris (Eds.), Photosynthetic Reaction Centers, Academic Press, New York, 1993, pp. 13–21.
[14] M. Wendling, M.A. Przyjalgowski, D. Gülen, S.I.E. Vulto, T.J. Aartsma, R. van Grondelle, H. van Amerongen, Photosynth. Res. 71 (2002) 99–123.
[15] H. van Amerongen, L. Valkunas, R. van Grondelle, Photosynthetic Excitons, World Scientific Publishers, Singapore, 2000.
[16] Th. Renger, V. May, O. Kühn, Phys. Rep. 343 (2001) 137–254.
[17] V. May, O. Kühn, Charge and Energy Transfer Dynamics in Molecular Systems, second ed., Wiley-VCH, Weinheim, 2003.
[18] B. Brüggemann, V. May, J. Chem. Phys. 120 (2004) 2325–2336.
[19] O. Kühn, V. Sundström, T. Pullerits, Chem. Phys. 275 (2002) 15–30.
[20] M. Wendling, T. Pullerits, M.A. Przyjalgowski, S.I.E. Vulto, T.J. Aartsma, R. van Grondelle, H. van Amerongen, J. Phys. Chem. B 104 (2000) 5825–5831.
[21] The backward propagation of the auxiliary density operator follows from a re-interpretation of the functional derivative of the observable to be optimized, here $P_m(t_f)$, with respect to $\mathbf{E}$. Originally, the derivative leads to an expression similar to Eq. (4) but with the trace written as $\mathrm{tr}\{|m\rangle\langle m|\mathcal{U}(t_f, t)[\hat{\mu}, \hat{\rho}(t; \mathbf{E})]\}$. Then, it becomes possible to rearrange the time-evolution superoperator $\mathcal{U}$ in such a way that it acts completely to the left, just propagating $|m\rangle\langle m|$ backwards in time.